Analysis of the Fading Channel in Downlinks from the Lunar South Pole to the Deep Space Network

Marc Sanchez Net*

ABSTRACT. — This article studies the fading channel between a grounded asset on the South Pole of the Moon and a DSN station utilizing a 34-meter antenna. Due to geometrical constraints in the Earth-Moon system, missions operating in the lunar South Pole will need to communicate with Earth by pointing their antennas at a maximum elevation angle of 10 degrees. This fact, combined with low gain antennas typically found on-board rovers and landers, will cause signal reflections with the Moon surface and create fading effects that are uncharacteristic of space applications. On the other hand, the receiving stations on Earth will utilize highly directional antennas, an uncommon situation in most systems suffering from fading effects (e.g.,, mobile communications).

Unfortunately, a complete characterization of the fading channel is not possible since no measurements of the scattering function and/or power delay profile at the South Pole of the Moon are currently available. Therefore, we study the channel properties from an analytic point-of-view assuming that it can be modeled as wide sense stationary process with uncorrelated scattering function. In particular, we derive expressions for the Doppler power profile, channel coherence time and average fade duration as a function of the receiving antenna directivity. Results indicate that, for missions transmitting at tens or hundreds of kilobits per second, the stochastic channel between the South Pole of the Moon and Earth exhibits slow fading. Furthermore, the time selectivity of the channel is directly related to the receiving antenna directivity and operating frequency.

---

*Communications Architectures and Research Section.

The research described in this publication was carried out by the Jet Propulsion Laboratory, California Institute of Technology, under a contract with the National Aeronautics and Space Administration.

I. Introduction

The South Pole of the Moon has recently gained attention as a potential area of interest to be explored in the near future. Indeed, it is thought that deposits of ice water might be available in constantly shaded areas of this region, a valuable resource that could be mined with *In-Situ Resource Utilization* technology to facilitate human exploration of the Moon and beyond. To validate this hypothesis, several robotic rovers destined for that region have been conceived and studied (e.g., Lunar Resource Prospector [1], Chandrayaan-2 [2]). Most of them have moderate or low data requirements, but their limited mass and power budgets require transmission to Earth using a low or medium directional antenna on the rover and a very large aperture on Earth (e.g., 34-meter Deep Space Network antenna).

Unfortunately, the geometry of the Earth-Moon system dictates that the maximum elevation angle of the rover antenna can never exceed 10 deg. This, coupled with the transmitter low directivity, results in the signal's Fresnel zone intersecting with the Moon surface and causes signal reflections that can add constructively or destructively at the receiver. In other words, the channel suffers from multi-path fading effects rarely encountered in space communications [3]. As a matter of fact, and to the best of the author's knowledge, this phenomena has only been problematic in the past in a handful of cases: Communications from the Apollo Lunar Module to Earth while in lunar orbit [4]; transmission of data during Extra Vehicular Activities in the International Space Station [5]; and missed reception of tones from the Mars Exploration Rover Spirit right after landing on a shallow depression [6].

To mitigate multi-path fading effects, several options are possible: increase the transmission power (or decrease the data rate) so that the link margin exceeds a certain threshold; utilize automatic gain control techniques; provide antenna diversity at the transmitter, receiver, or both; use interleavers to spread errors across multiple codewords; provide redundancy at a higher layer through Automatic Repeat reQuest mechanisms; or even open-loop recording of the received signal for ground processing and radio science applications. Understanding which of these alternatives to implement requires knowledge about the channel conditions to be expected. On Earth, this can be done experimentally by taking measurements of channel properties such as the power delay profile (PDP) and Doppler power profile (DPP). Unfortunately, no such measurements exist (or can be easily gathered) from the South Pole of the Moon. Therefore, we study the fading channel from a theoretical point of view under the assumption that a highly directive antenna (i.e., a DSN 34-meter dish) is used at the receiver, and the fading process is uncorrelated and wide sense stationary. In particular, we first provide approximations for the Doppler power profile as a function of the antenna directivity at the receiver. This result is then used to infer the channel time selectivity, specifically its coherence time and average fade duration. This allows us to characterize the channel as a slow fading process with fades that last between three and six orders of magnitude longer than common fading channels.

Finally, the frequency selectivity of the fading channel between the South pole of the Moon and a DSN station is not properly studied in this article since power Delay profile measurements are not available. In that sense, the best we can do is hypothesize the channel conditions by analogy with Earth measurements. For instance, power Delay profile measurements in desert-like environments on Earth indicate that the expected delay spread is typically lower than $0.5\mu s$ [7], and therefore the coherence bandwidth is greater than 2 MHz. Since missions like the Resource Prospector will transmit at tens or hundreds of kilobits per second, it seems reasonable to assume that the channel will suffer from flat fading conditions. However, further research is required to validate this statement.

II. System and Channel Model Description

We consider a two-dimensional model of the system as depicted in Figure 1. The DSN antenna moves along the x-direction with velocity $\vec{\mathbf{v}}$ due to Earth's rotation while tracking the stationary transmitter on the South Pole of the Moon [8]. Furthermore, we let θ_0 denote the direct line-of-sight (LoS) direction between transmitter and receiver as measured from $\vec{\mathbf{v}}_\mathbf{x}$[2].

Multiple reflected copies of the signal transmitted by the rover on the lunar South Pole arrive at the DSN station, each of them with a different delay τ_n and from a slightly different direction θ_n (also measured from $\vec{\mathbf{v}}_\mathbf{x}$). Both delay and direction depend on the set of reflections a given ray has encountered on its path from origin to destination which, in turn, is a function of the lunar South Pole topography. Rays arriving from direction θ_n experience a Doppler shift proportional to the Earth rotation speed, $\nu_n = \frac{\|\vec{\mathbf{v}}_\mathbf{x}\|}{c}\nu_c \cos\theta_n$, where c is the speed of light and ν_c denotes the

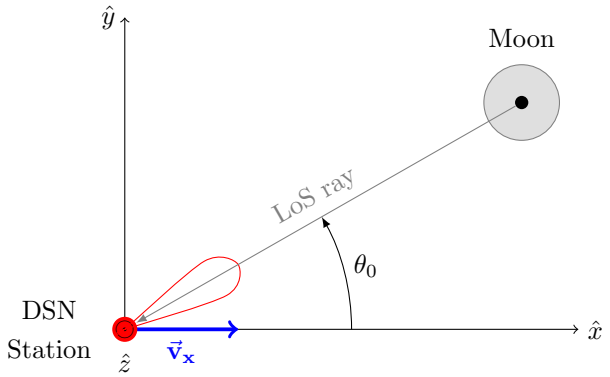

Figure 1. System Geometry (Top View)

[2]The reference frame $(\hat{x}, \hat{y}, \hat{z})$ is chosen such as that $\hat{x}$ is tangent to Earth's surface and aligned with its rotation vector, $\hat{z}$ is the zenith direction, and $\hat{y}$ completes the right-handed coordinate system. Since the Moon orbit is not perfectly circular, $\vec{\mathbf{v}}$ will also have a small component on the $\hat{y}$ direction, but in this paper we assume its effect to be negligible.

carrier frequency. Therefore, the fading channel is, in general, both time and frequency dispersive (or equivalently, frequency and time selective) and can be modeled using a linear time-varying (LTV) filter [9]:

$$r(t) = h(t,\tau) * s(t) + n(t), \tag{1}$$

where $*$ denotes the convolutional operator

$$h(t,\tau) * s(t) = \int_{-\infty}^{\infty} h(t,\tau)s(t-\tau)d\tau, \tag{2}$$

$s(t)$ and $r(t)$ are the complex baseband equivalents of the transmitted and received signal respectively, $h(t,\tau)$ is the channel time-varying impulse response, and $n(t)$ is complex additive white Gaussian noise (AWGN) assumed to be negligible for the rest of this discussion.

The received complex envelope can be approximated as the sum of all rays arriving at the receiver at any given point in time:

$$r\left(t\right) = \sum_{n=0}^{N} C_n e^{-j\phi_n} s\left(t-\tau_n\right) e^{j2\pi\nu_n t}, \tag{3}$$

where τ_n is the delay experienced by the n-th ray, and C_n and $\phi_n = 2\pi(\nu_c + \nu_n)\tau_n$ denote its attenuation and phase delay, respectively [8]. In other words, we utilize a discrete model of the world where the channel can be expressed as

$$h(t,\tau) = \sum_{n=0}^{N} h_n \delta\left(\tau-\tau_n\right) e^{j2\pi\nu_n t}, \tag{4}$$

where $\delta(x)$ indicates the Dirac delta function and $h_n = C_n e^{-j\phi_n} \in \mathbb{C}$ models the channel response that the n-th ray experiences given the direction/delay with which it arrives at the receiver.

Taking the Fourier transform with respect to the time variable results in the channel *spreading function*, which fully characterizes the channel time and frequency selectivity [9]:

$$\begin{aligned} S(\tau,\nu) &= \int_{\infty}^{\infty} h(t,\tau)e^{-j2\pi\nu t}dt \\ &= \sum_{n=0}^{N} h_n \delta\left(\tau-\tau_n\right) \int_{\infty}^{\infty} e^{-j2\pi(\nu-\nu_n)t}dt \\ &= \sum_{n=0}^{N} h_n \delta\left(\tau-\tau_n\right)\delta\left(\nu-\nu_n\right). \end{aligned} \tag{5}$$

Observe that in the case of a channel with a discrete number of rays arriving at the receiver, the spreading function is equal to a set of deltas in the (τ,ν)-plane, each of which is weighted by a complex factor h_n. In the limit, however, a channel with an infinite number of rays arriving from all directions and with all delays is possible. Therefore, $S(\tau,\nu)$ would be a complex continuous surface of arbitrary shape.

A. Simplified Stochastic Channel Model

In real-life systems the channel impulse response (or equivalently, its spreading function) is not known by the transmitter and receiver, and is not necessarily constant. Therefore, it is modeled as a stochastic random process. For instance, let us consider the discretized spreading function from Equation 5. Assume also that the number of rays incident on the receiver at any point in time is large ($N \to \infty$). Then we can invoke the Central Limit Theorem and argue that $S(\tau, \nu)$ will converge to a 2D complex Gaussian random process. To characterize it, we assume it has zero mean and estimate its autocorrelation function (ACF) as

$$\phi_s(\tau, \nu; \tau', \nu') = E\left\{S(\tau, \nu) S^*(\tau', \nu')\right\}. \tag{6}$$

In other words, if we know $\phi_s(\tau, \nu; \tau', \nu')$ then we can in theory create random realizations of the channel spreading function $S(\tau, \nu)$ and, from those, compute samples of the channel impulse response $h(t, \tau)$. This is analogous to being able to obtain normally distributed samples given mean and variance in a Monte Carlo experiment.

Clearly the scattering function as described by Equation 6 is too general to be applied directly to any engineering problem unless measurements of the specific channel under consideration are available (see Reference [10] for an example with two vehicles traveling in opposite directions). As previously mentioned, this is not possible in our application and, therefore, further simplifications and assumptions must be made. In that sense, it is customary to assume that the channel is wide sense stationary with uncorrelated scattering (WSSUS).

It can be shown that in WSSUS channels both the Doppler and delay coefficients are uncorrelated with each other [9]. Therefore, the spreading function's ACF can be simplified to

$$\phi_s(\tau, \nu; \tau', \nu') = C_h(\tau, \nu)\delta(\tau - \tau')\delta(\nu - \nu'), \tag{7}$$

where $C_h(\tau, \nu)$ is known as the scattering function and dictates the properties of the fading channel 2D Gaussian process. Note that, intuitively, the WSSUS assumption is somewhat unnatural. Indeed, rays suffering approximately the same delay and Doppler shift have probably followed a similar set of reflections to the receiver and, therefore, should have experienced similar channel conditions (i.e., they should be correlated). However, experimental results in mobile communications have validated this simplification usefulness, so much so that well-known standards such 3GPP and LTE use it in their tapped-delay line channel models [11], [12].

Finally, it is also common practice to consider the scattering function as separable into its delay and Doppler contributions:

$$C_h(\tau, \nu) = C_{h_1}(\tau) C_{h_2}(\nu), \tag{8}$$

where $C_{h_1}(\tau)$ is known as the *power delay profile* (PDP) and $C_{h_2}(\nu)$ denotes the *Doppler power profile* (DPP). In other words, $C_{h_1}(\tau)$ characterizes the frequency

selectivity of the channel, while $C_{h_2}(\nu)$ determines its time selectivity. As an example, a commonly used fading channel assumes the DPP profile of a 2D isotropic scattering environment combined with an exponentially decaying PDP [9]:

$$C_{h_1}(\tau) \propto \frac{1}{\tau_0} e^{-\tau/\tau_0} \tag{9}$$

$$C_{h_2}(\nu) \propto \frac{1}{\pi \nu_m \sqrt{1-(\nu/\nu_m)^2}}, \tag{10}$$

where $C_{h_1}(\tau)$ is defined for $\tau \geq 0$ and 0 otherwise, $C_{h_2}(\nu)$ is valid for $|\nu| < \nu_m$ and 0 otherwise, and $\nu_m = v/\lambda_c$ is the maximum Doppler frequency in the system.

B. Doppler Power Profile

To compute a fading channel's DPP, we go back to the discrete model (see Equation 3) and assume that the transmitter sends a single tone at the carrier frequency (i.e., $s(t) = 1$). Then, the received complex envelope can be expressed in terms of the in-phase and quadrature components as [8]

$$r\,(t) = r_I(t) + j r_Q(t), \tag{11}$$

where, by the Central Limit Theorem,

$$r_I(t) = \sum_{n=0}^{N} C_n \cos(\phi_n - \nu_n t) \sim \mathcal{N}\,(0, b_0) \tag{12}$$

$$r_Q(t) = \sum_{n=0}^{N} C_n \sin(\phi_n - \nu_n t) \sim \mathcal{N}\,(0, b_0)\,, \tag{13}$$

with $b_0 = \frac{1}{2}\sum_{n=0}^{N} C_n^2$ denoting the variance of the real and imaginary parts of the complex stochastic process (or, equivalently, $2b_0$ is the total received envelope power for the complex baseband signal). Furthermore, neither $r_I(t)$ nor $r_Q(t)$ are independently distributed from $r_I(t')$ and $r_Q(t')$. Instead, given that the channel is WSSUS and assuming that the scattering function is separable, the autocorrelation function is simply

$$\phi_{rr}(\tau) = \phi_{II}\,(\tau) + j\phi_{IQ}\,(\tau)\,, \tag{14}$$

where $\tau = t' - t$ and

$$\phi_{II}\,(\tau) = E_{\tau,\theta}\left\{r_I(t) r_I(t+\tau)\right\} = b_0 E_\theta\left\{\cos\left(2\pi\nu_m \tau \cos\theta\right)\right\} \tag{15}$$

$$\phi_{IQ}\,(\tau) = E_{\tau,\theta}\left\{r_I(t) r_Q(t+\tau)\right\} = b_0 E_\theta\left\{\sin\left(2\pi\nu_m \tau \cos\theta\right)\right\}. \tag{16}$$

Following [8], we have assumed that the phase delay of the received rays ϕ_n is uniformly distributed in $[-\pi, \pi]$ and ν_m is maximum Doppler shift.

Let $p(\theta)G(\theta)$ denote the set of directions through which a ray can arrive at the receiver weighted by the gain of the receiving antenna in that direction. Assume also that $p(\theta)G(\theta)$ is normalized so that its integral is equal to 1 and it is a pair function

(i.e., the antenna gain pattern exhibits symmetry with respect to the boresight direction). Then,

$$\phi_{II}(\tau) = b_0 \int_{\theta_{min}}^{\theta_{max}} \cos(2\pi\nu_m \tau \cos\theta) p(\theta) G(\theta) d\theta, \tag{17}$$

$$\phi_{IQ}(\tau) = b_0 \int_{\theta_{min}}^{\theta_{max}} \sin(2\pi\nu_m \tau \cos\theta) p(\theta) G(\theta) d\theta, \tag{18}$$

Let us now consider the following change of variables $\varphi = \theta - \theta_0$. Then, if the receiving antenna is pointed and tracking the transmitter, φ measures the angle between the antenna's boresight direction and the direction through which a ray arrives at the receiver. Furthermore, let us also define $\xi = \tau\nu_v$ as the Doppler normalized delay. Then,

$$\phi_{rr}(\xi) = b_0 \int_{\varphi_{min}}^{\varphi_{max}} e^{j2\pi\xi\cos(\varphi+\theta_0)} p(\varphi) G(\varphi) d\varphi. \tag{19}$$

and the channel DPP $C_{h_2}(\nu)$ is simply computed by taking its Fourier Transform[3].

As an example, consider the case of 2D isotropic scattering; i.e., the receiver uses an omnidirectional antenna and rays can arrive from any direction. Then, $p(\theta)G(\theta) = \frac{1}{2\pi}$, which yields [8]

$$\phi_{rr}(\xi) = b_0 J_0(2\pi\xi) \tag{20}$$

$$C_{h_2}(f) = \begin{cases} \frac{b_0}{\pi} \frac{1}{\sqrt{1-f^2}} & |f| \leq 1 \\ 0 & \text{otherwise,} \end{cases} \tag{21}$$

with $f = \nu/\nu_m$ and $J_0(x)$ equal to the zero-order Bessel function of the first-kind. Note that $C_{h_2}(f)$ is the same as in Equation 10 but using the normalized frequency domain.

C. Rayleigh vs. Rician Fading

When the fading environment is non-isotropic, certain preferential directions concentrate most of the received power. The simplest form of non-isotropic fading is generated by superimposing 2D isotropic scattering plus a single dominant LoS ray. Therefore, the complex baseband equivalent of the received signal can be expressed as

$$r(t) = r_I(t) + j r_Q(t), \tag{22}$$

[3]Note that if ξ is used in the Fourier transform, then the resulting expression will be in terms of $f = \nu/\nu_m$.

where

$$r_I(t) = s\cos(2\pi\nu_0 t) + \sum_{n=0}^{N} C_n \cos(\phi_n - \nu_n t) \sim \mathcal{N}(s(t), b_0) \tag{23}$$

$$r_Q(t) = s\sin(2\pi\nu_0 t) + \sum_{n=0}^{N} C_n \sin(\phi_n - \nu_n t) \sim \mathcal{N}(s(t), b_0), \tag{24}$$

with $\nu_0 = \nu_m \cos\theta_0$. Similarly, the distribution of incident power on the receiver can becomes

$$p(\theta)G(\theta) = \frac{1}{K+1} p_s(\theta)G(\theta) + \frac{K}{K+1}\delta(\theta - \theta_0)G(\theta_0), \tag{25}$$

where $p_s(\theta)$ is the angle of arrival distribution for just the scattered component and K is equal to the ratio of LoS and scattered power (known as the *Rice factor*).

Based on this, it can be shown that the received signal envelope $\alpha(t) = |r(t)|$ is in general Rician distributed with parameters s^2 and $2b_0$, where s^2 is the power of the direct LoS ray and $2b_0$ is the scattered power ($\Omega_p = s^2 + 2b_0$, $K = s^2/2b_0$) [8]. Furthermore, if we assume that the LoS and scattered rays arrive at the receiver with independent phases, and the receiver antenna exhibits symmetry with respect to its boresight direction, then

$$\phi_{II}(\xi) = \frac{1}{K+1}\frac{\Omega_p}{2}\phi_{II}^{(s)}(\xi) + \frac{K}{K+1}\frac{\Omega_p}{2}\cos(2\pi\xi\cos\theta_0) \tag{26}$$

$$\phi_{IQ}(\xi) = \frac{1}{K+1}\frac{\Omega_p}{2}\phi_{IQ}^{(s)}(\xi) + \frac{K}{K+1}\frac{\Omega_p}{2}\sin(2\pi\xi\cos\theta_0), \tag{27}$$

where $\phi_{rr}^{(s)}(\xi)$ is the normalized autocorrelation function of the channel's scattered component[4]. Similarly, the channel DPP will be equal to

$$C_{h_2}(\nu) = \frac{1}{K+1}\frac{\Omega_p}{2}C_{h_2}^{(s)}(\nu) + \frac{K}{K+1}\frac{\Omega_p}{2}\delta(\nu - \nu_m\cos\theta_0), \tag{28}$$

where $C_{h_2}^{(s)}(\nu)$ is the normalized DPP of the scattered component and the rest is introduced by the LoS ray. Finally, if there is no dominant LoS ray, i.e., $K = 0$, then the channel is said to suffer from Rayleigh fading, a condition that had been implicitly assumed in previous sections.

D. Antenna Model and Approximations

In Section II-B we have shown that the channel DPP depends on the gain of the receiving antenna. In most applications (e.g., cellphones), an omnidirectional antenna is used and, consequently, Equation 21 can be used to model the channel's frequency response. However, this is not always the case. In some microcell applications for densely urban areas, it is sometimes assumed that rays are channeled by buildings and, therefore, concentrate their angle of arrival in a preferential direction [8]. Similarly, in

[4]For instance, $\phi_{rr}^{(s)}(\xi)$ for 2D isotropic scattering is obtained from Equation 20 when $b_0 = 1$.

the case of the DSN it is clear that assuming omnidirectional antennas at the receiver is not realistic. Therefore, the fading channel DPP needs to be reevaluated.

The exact gain pattern of a DSN antenna depends primarily on whether the receiver is located in the near, mid, or far field. Jamnejad provides in Reference [13] detailed expressions for the thresholds between these three regions as a function of the antenna size, operating frequency, and distance to the transmitter. He also provides specific equations to characterize the gain of a DSN antenna depending on the off-axis angle φ. For the purposes of this paper, it is obvious that the DSN antennas will operate in the far field region given the distance from the South Pole of the Moon and Earth. If that is the case, the gain of a parabolic antenna can be approximated as

$$G(\varphi) = \eta \left(\frac{\pi D}{\lambda_c}\right)^2 \left(\frac{1+\cos\varphi}{2\cos\varphi}\right)^2 \Lambda_1^2 \left[\left(\frac{\pi D}{\lambda_c}\right)\tan\varphi\right], \tag{29}$$

where D is the antenna diameter, λ_c is the carrier wavelength, η is an efficiency factor to account for feed spillover, polarization and other losses, and $\Lambda_1[x]$ is the normalized Bessel function or Lambda function of the first order [13]. Note that this equation assumes a reflector with perfect symmetry. In reality, wind loading effects and mechanical deformations of large parabolic antennas can break this symmetry and distort the gain pattern, but we obviate these second-order effects for now.

Other gain patterns for highly directive antennas at the receiver are possible. In particular, two alternatives are considered, the ITU-R average radiation model [14], and an exponentially decaying gain of the form

$$G(\varphi) = G_{max} e^{-k\varphi^2}. \tag{30}$$

Note that the main lobe of the radiation pattern for both a DSN antenna and the ITU-R model decay exponentially with the off-axis angle [15], [14]. Therefore, the proposed exponential radiation pattern is essentially an approximation by which only the main lobe is considered. In that sense, if the antenna is highly directive, its gain will typically be approximately two orders of magnitude (20 dB) larger than the secondary lobes, and therefore the approximation will be valid. Also, from Reference [15] we know that for a DSN antenna $k = \frac{2.773}{HPBW^2}$, where $HPBW$ is the half-power beamwidth. Similarly, it is well-known that the half-power beamwidth of a parabolic antenna is approximately equal to $a(\lambda/D)$, where a is an dimensionless constant that depends on the antenna illumination efficiency. Therefore, we conclude that the parameter k will increase quadratically with both the diameter of the antenna and the carrier frequency:

$$k \approx \frac{2.773}{(a\frac{\pi}{180}c)^2}(\nu_c D)^2, \tag{31}$$

where c is the speed of light (in general, $a \approx 70$ [16], but for the 34-m DSN antennas experimental data suggests that $a \approx 63.25$ [15]).

Figure 2 compares the radiation pattern of a 1-m parabolic dish and a 34-m DSN antenna operating at X-band estimated with Equation 29, the ITU-R model, and an

exponential fit. For the ITU-R model, the antenna diameter is set to 1 and 34-meters, respectively, to make a fair comparison. For the latter, the decaying parameter k is estimated based on Equation 31. Observe that the exponential approximation is quite accurate until the gain falls below -17.5 dB approximately, at which point the secondary lobes become dominant. However, the contribution of rays arriving through these secondary lobes will be attenuated by almost two orders of magnitude as compared to the LoS ray, and therefore will have negligible effect on the receiver. Consequently, for the rest of the paper we will assume an exponentially decaying radiation pattern to characterize the fading channel process analytically, but numerical results with the actual DSN radiation pattern will be provided for comparison purposes.

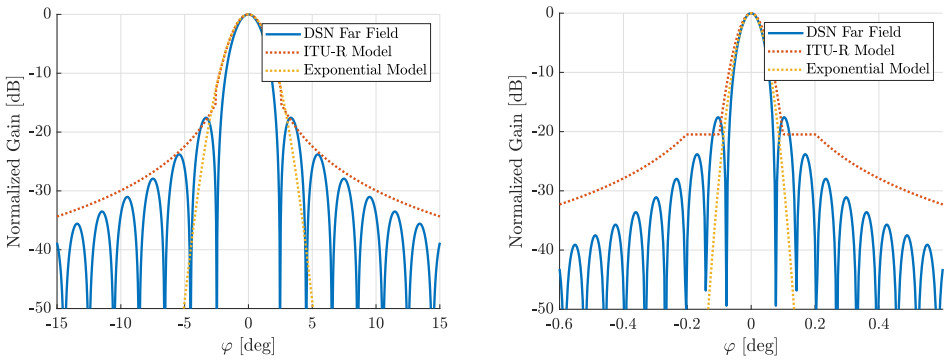

(a) 1-m Parabolic Antenna **(b) 34-m DSN Antenna**

Figure 2. Comparison of Radiation Patterns Models

III. Fading Channel Autocorrelation and Doppler Power Profile

In this section we derive the channel autocorrelation function for the scattered component of the fading channel between the South Pole of the Moon and a DSN station. Then, we provide analytic expressions for the channel DPP. All equations assume a highly directive antenna such that its radiation pattern can be successfully approximated with an exponentially decaying model with characteristic parameter k. Finally, it is assumed that scattered rays can be collected at the DSN antenna if they arrive within ± 90 deg of the antenna boresight direction. As we will see, this assumption becomes inconsequential in the case of highly directional antennas.

Lemma 1. *Assume that* $p(\varphi) = 1/(2\Phi)$, $\varphi \in [-\Phi, \Phi]$, *and* $G(\varphi) = e^{-k\varphi^2}$, *and let* $\xi = f_m \tau$ *be the time lag normalized by the maximum Doppler frequency. Assume also that the antenna is highly directive, i.e.,* $k \gg 1$. *Then the scattered component of the*

fading channel autocorrelation function can be approximated as

$$\phi_{rr}^{(s)}(\xi) \approx \begin{cases} b_0 e^{-\frac{(\pi\theta_0\xi)^2}{k}+j2\pi\xi\cos\theta_0} & \theta_0 \to 0 \\ b_0 e^{-\frac{(\pi\xi)^2}{k}+j2\pi\xi\cos\theta_0} & \theta_0 \to \frac{\pi}{2}. \end{cases} \tag{32}$$

The proof is given in Appendix A.

Observe that Equation 32 does not depend on Φ. Indeed, if the antenna has high directivity then its radiation pattern will be the primary factor to limit the directions through which a ray can reach the receiver.

Corollary 1.1. *Under the assumptions of Lemma 1, the fading channel DPP is*

$$C_{h_2}^{(s)}(f) \approx \begin{cases} b_0\delta(f-1) & \theta_0 = 0 \\ \frac{b_0}{\theta_0}\sqrt{\frac{k}{\pi}}e^{-\frac{k}{\theta_0^2}(f-\cos\theta_0)^2} & \theta_0 \to 0 \\ b_0\sqrt{\frac{k}{\pi}}e^{-k(f-\cos\theta_0)^2} & \theta_0 \to \frac{\pi}{2}. \end{cases} \tag{33}$$

The proof is given in Appendix B. Observe that the Channel DPP is normalized such that $\int_{-1}^{1} C_{h_2}^{(s)}(f) = \phi_{rr}^{(s)}(0) = b_0$ *as expected.*

Corollary 1.2. *Under the assumptions of Corollary 1.1 and for* $\theta \neq 0$*, the fading channel DPP is Gaussian distributed:*

$$C_{h_2}^{(s)}(\nu) \approx \frac{b_0}{\sqrt{2\pi}\sigma_\nu} e^{-\frac{(\nu-\nu_0)^2}{2\sigma_\nu^2}} \tag{34}$$

with $\nu_0 = \nu_m \cos\theta_0$ *and*

$$\sigma_\nu = \begin{cases} \frac{\nu_m\theta_0}{\sqrt{2k}} & \theta_0 \to 0 \\ \frac{\nu_m}{\sqrt{2k}} & \theta_0 \to \frac{\pi}{2}. \end{cases} \tag{35}$$

The proof follows from Corollary 1.1 using the unnormalized frequency domain $\nu = f\nu_m$ *and directly substituting* σ_ν *into* $C_{h_2}^{(s)}(\nu)$*.*

Finally, we substitute the values for ν_m and k into the channel DPP standard deviation and obtain that

$$\sigma_\nu \approx \begin{cases} \alpha\frac{\|\vec{\mathbf{v}}_\mathbf{x}\|\theta_0}{D} & \theta_0 \to 0 \\ \alpha\frac{\|\vec{\mathbf{v}}_\mathbf{x}\|}{D} & \theta_0 \to \frac{\pi}{2} \end{cases}, \tag{36}$$

where $\vec{\mathbf{v}}_\mathbf{x}$ is defined in Figure 1, D denotes its diameter and the factor $\alpha \in [0.468, 0.518] \approx 0.5$ is an experimental constant that depends on its illumination efficiency.

A. Comparison of Approximations vs. Numerical Results

To validate the provided approximations we estimate the channel autocorrelation function and DPP numerically from the gain antenna pattern in Equation 29 assuming

that the antenna is pointed at an angle $\theta_0 = 115$ deg[5] and operates at X-band ($f_c = 8.45$ GHz). The experiment is first run for a 1-m parabolic dish and then for a 34-m DSN antenna. For reference, we also provide the results for the ITU-R average model.

Figure 3 compares the in-phase component of the autocorrelation function for the three cases considered. Observe that both the analytic model and ITU-R model slightly underestimate the level of autocorrelation due to the radiation pattern secondary lobes. However, if the antenna used at the receiver is a 1-m dish, then the channel will exhibit correlation for approximately 30 lags in all three cases. In contrast, if the 34-m DSN antenna is utilized, then the channel will be correlated for up to 1000 lags.

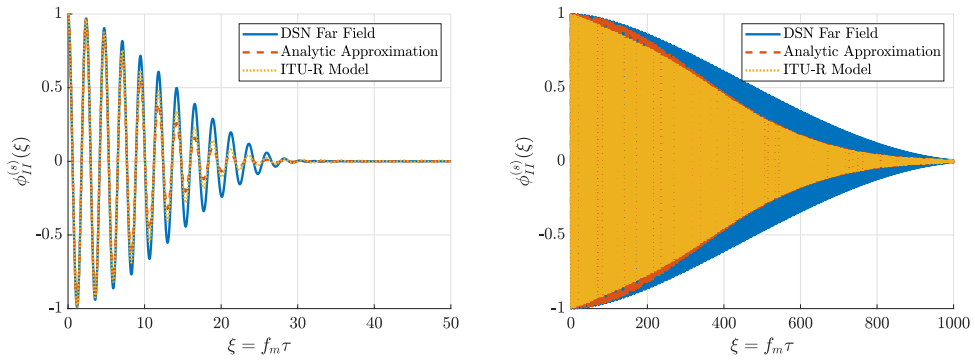

(a) 1-m Parabolic Antenna **(b) 34-m DSN Antenna**

Figure 3. Fading Channel Autocorrelation Function

Figure 4 compares the DPP function for the same three radiation patterns. For the DSN far field and ITU-R model, the DPP has been obtained numerically by applying the Fast Fourier Transform (FFT) over the autocorrelation function from Figure 3. Therefore, the resulting plots are subject to windowing effects that do not affect the analytic expression from Corollary 1.1. Observe that the peak of the DPP function is correctly placed at $f = \cos\theta_0$ in both the 1-m and 34-m antennas. Furthermore, the peak's width is inversely related to the antenna directivity, a fact that once again indicates larger channel autocorrelation.

B. Comparison with 2D Isotropic Scattering

We now compare the autocorrelation function and DPP of a fading channel with an omnidirectional antenna (2D isotropic scattering), a 1-m parabolic dish, or a 34-m DSN antenna at the receiver. For the omnidirectional antenna, θ_0 is irrelevant since rays can be collected through any direction. In contrast, for the directive antennas two cases are presented, one for $\theta_0 = 90\,\text{deg}$ and another one for $\theta_0 = 115\,\text{deg}$. Note that in

[5]This is is the maximum angle experienced in the channel between the South Pole of the Moon and a DSN station.

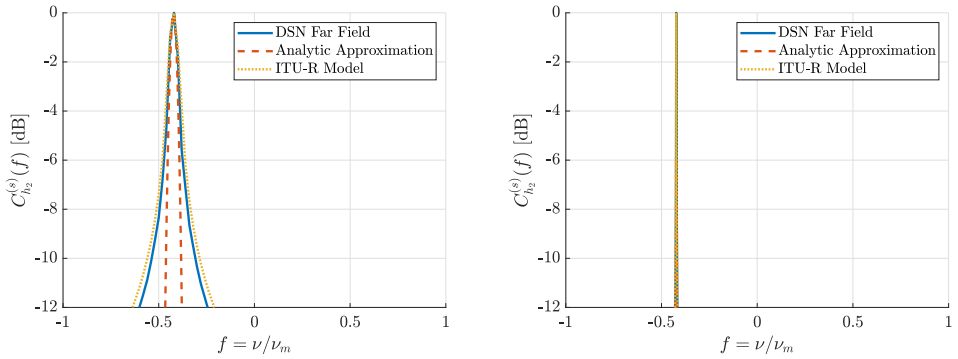

(a) 1-m Parabolic Antenna **(b) 34-m DSN Antenna**

Figure 4. Fading Channel Doppler Power Profile

the former case most of the rays will not suffer any Doppler shift since the DSN velocity vector is perpendicular to them.

Figure 5 show the results of the channel autocorrelation analysis. Consistent with previous results, the autocorrelation function decays significantly faster in the case of the 1-m antenna. However, this exponential decay is still significantly slower than the Bessel function characteristic of an omnidirectional antenna. This fact, in turn, is also observable in the channel DPP presented in Figure 6. Indeed, the typical U-shaped form of a 2D isotropic scattering channel DPP is significantly wider than the peaks centered around $f = \cos\theta_0$.

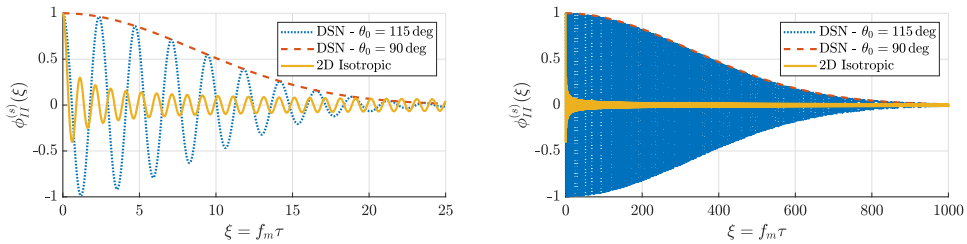

(a) 1-m Parabolic Antenna **(b) 34-m DSN Antenna**

Figure 5. Fading Channel Autocorrelation Function

Finally, note that the obtained relationship between antenna gain, channel autocorrelation function, and DPP makes sense from a physical standpoint. Indeed, an infinitely directive antenna would have a gain pattern equal to a delta in the θ_0 direction. Therefore, only the LoS ray would be received and the channel autocorrelation function would be a single tone[6]. Therefore, the DPP would be equal to a delta around $\nu = \nu_m \cos\theta_0$.

[6]Recall here that the autocorrelation function of a cosine is also a cosine.

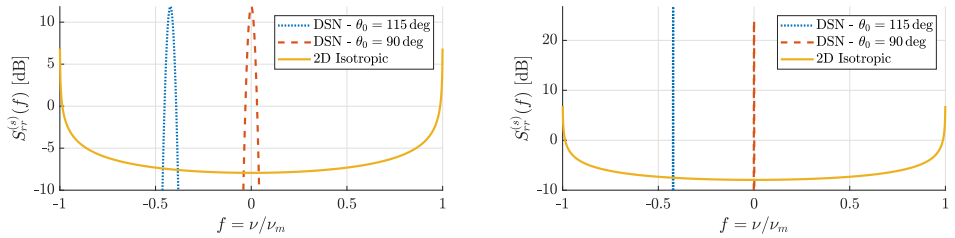

(a) 1-m Parabolic Antenna **(b) 34-m DSN Antenna**

Figure 6. Fading Channel Doppler Power Profile

IV. Fading Channel Coherence Time

The coherence time T_c of a fading channel measures the time selectivity of its impulse response. It is typically compared against the symbol duration to differentiate between slow and fast fading. As an example, consider a channel that is only time selective and assume that $T_c \leq T_s$. Then, the channel is said to experience fast fading and its impulse response can be approximately modeled as

$$h(t,\tau) \approx \sum_{n=0}^{N} h_n(t) e^{j2\pi\nu_n t}\delta(\tau) = h(t)\delta(\tau), \tag{37}$$

where $h(t) \in \mathbb{C}$ is a stochastic process that varies rapidly within a symbol period. In other words, the complex baseband equivalent of the received signal is equal to

$$r(t) = h(t,\tau) * s(t) = \int_{-\infty}^{\infty} h(t)\delta(\tau)s(t-\tau)d\tau = h(t)s(t). \tag{38}$$

On the other hand, if $T_c \gg T_s$ then the channel is said to experience slow fading. In that case, $h(t)$ varies slowly within a symbol time and, therefore, the channel impulse response can be approximated as

$$h(t,\tau) \approx h\delta(\tau), \tag{39}$$

with $h \in \mathbb{C}$ constant[7]. Therefore, from the point of view of demodulation and decoding, the channel introduces a constant fade and phase shift as dictated by h's absolute value and angle.

For a generic WSSUS channel, the coherence time can be estimated as $T_c = \frac{1}{\sigma_\nu}$, where σ_ν is the *Doppler spread* of the scattering function:

$$\sigma_\nu^2 = \frac{1}{b_0}\int_{-\infty}^{\infty}\int_{-\infty}^{\infty}(\nu-\bar{\nu})^2 C_h(\tau,\nu)d\tau d\nu. \tag{40}$$

[7]This mathematical definition comes from Reference [9]. Other authors define the coherence time as an experimentally determined constant divided by the maximum Doppler shift.

In turn, $\bar{\nu}$ is the expected average Doppler shift experienced by all rays collected by the receiver's aperture:

$$\bar{\nu} = \frac{1}{b_0} \int_{-\infty}^{\infty} \int_{-\infty}^{\infty} \nu C_h(\tau, \nu) d\tau d\nu. \tag{41}$$

Let us also assume again that the spreading function is separable. Then,

$$\sigma_\nu^2 = \frac{1}{b_0} \int_{-\infty}^{\infty} (\nu - \bar{\nu})^2 C_{h_2}(\nu) d\nu \tag{42}$$

$$\bar{\nu} = \frac{1}{b_0} \int_{-\infty}^{\infty} \nu C_{h_2}(\nu) d\nu. \tag{43}$$

Lemma 2. *Assume that $p(\varphi) = 1/(2\Phi)$, $\varphi \in [-\Phi, \Phi]$, and $G(\varphi) = e^{-k\varphi^2}$, $k \gg 1$. Assume also that the fading channel is WSSUS and has a separable scattering function. Then,*

$$T_c \approx \begin{cases} \frac{\sqrt{2k}}{\nu_m \theta_0} & \theta_0 \to 0 \\ \\ \frac{\sqrt{2k}}{\nu_m} & \theta_0 \to \frac{\pi}{2}, \end{cases} \tag{44}$$

in units of seconds. The proof is given in Appendix C. Note also that T_c is the inverse from σ_ν in Equation 1.2 as expected.

Therefore, the channel coherence time will be inversely proportional to the Doppler shift experienced by the link between a spacecraft and a ground station. Furthermore, it will scale proportionally to the antenna diameter: $T_c \propto D$.

Corollary 2.1. *Under the assumptions of Lemma 2,*

$$T_c \approx \begin{cases} \frac{\sqrt{k}}{\theta_0} \cdot T_{c,2D} & \theta_0 \to 0 \\ \\ \sqrt{k} \cdot T_{c,2D} & \theta_0 \to \frac{\pi}{2}, \end{cases} \tag{45}$$

where $T_{c,2D}$ is the coherence time of fading channel with 2D isotropic scattering. The proof follows directly from the fact that $T_{c,2D} = \frac{\sqrt{2}}{\nu_m}$ [9].

Figure 7 provides numerical results for the normalized expected channel coherence time assuming an X-band WSSUS fading channel and 34-meter DSN antenna at the receiver. Three plots are provided: The channel coherence time valid for $\theta_0 \to \frac{\pi}{2}$ and $\theta_0 \to 0$, and the channel coherence time estimated as the maximum between these two values. Observe that the coherence time tends to infinity as θ_0 approaches zero since the PPD degenerates to a delta. On the other hand, when θ_0 is close to 90 deg, then the PPD has a single peak with maximum width, i.e., the autocorrelation function decreases faster and, therefore, the channel coherence time is shorter.

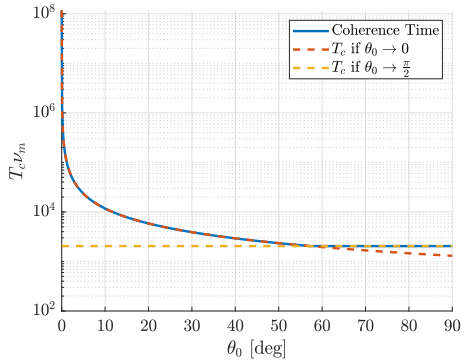

Figure 7. Fading Channel Coherence Time

Finally, for the Earth-Moon system, orbital propagation results indicate that $\theta_0 \in [70, 115]$ deg approximately and $\nu_m = 35$ kHz. Therefore, the coherence time can be estimated using the approximation for $\theta_0 \to \frac{\pi}{2}$ and results in a value of 58.4 msec. Furthermore, if we assume that a rover on the surface of the Moon transmits at rates between 1 kbps and 500 kbps, then the symbol duration time varies between 1 msec and 2 μsec and, therefore, the channel will suffer from very slow fading. In fact, we expect the link to experience effects akin to block fading channels, where a block of M consecutive symbols are affected by a channel impulse response that is strongly correlated or even constant. Furthermore, at any point in time the channel state will be dictated by the behavior of a 2D Gaussian process with autocorrelation given by Equation 32. Consequently, adjacent blocks of M symbols will not see uncorrelated channel conditions.

V. Level Crossing Rate and Average Fade Duration

In this section, we study second-order statistics of the channel stochastic process. In particular, we provide expressions for the level crossing rate and average fade duration (AFD) as a function of the channel's scattering function. To initiate the discussion, let us first recall that Rice's Formula can be used to count the number times a stationary process crosses a fixed level per unit of time in either the positive or negative direction [8]. It states that

$$L(R) = \int_0^\infty \dot{\alpha} p(\alpha = R, \dot{\alpha}) d\dot{\alpha}, \tag{46}$$

where $\alpha(t)$ is the signal envelope, $\dot{\alpha}(t)$ is its time derivative, and $p(\alpha, \dot{\alpha})$ is their joint probability density function. Rice also derived in [17] this last quantity for a sine wave (i.e., the LoS ray) plus narrow-band Gaussian noise (i.e., the scattered rays):

$$p(\alpha, \dot{\alpha}) = \frac{\alpha (2\pi)^{-3/2}}{\sqrt{B b_0}} \int_{-\pi}^{\pi} \exp\left[-\frac{B\left(\alpha^2 - 2\alpha s \cos\psi + s^2\right) + \left(b_0 \dot{\alpha} + b_1 s \sin\psi\right)^2}{2 B b_0} \right] d\psi, \tag{47}$$

where s^2 and b_0 are the Rician distribution parameters as defined in Section II-C, $B = b_0 b_2 - b_1^2$, and b_1 and b_2 are constants that, for a WSSUS fading channel with separable scattering function, depend only on the channel DPP [9], [17]:

$$\begin{aligned} b_n =&(2\pi)^n \int_{-f_m}^{f_m} C_{h_2}^{(s)}(\nu) \left[\nu - \nu_m \cos\theta_0\right]^n d\nu \\ =&(2\pi\nu_m)^n b_0 \int_{\theta_{min}}^{\theta_{max}} p_s(\theta) G(\theta) \left[\cos\theta - \cos\theta_0\right]^n d\theta, \end{aligned} \tag{48}$$

with $p_s(\theta)G(\theta)$ normalized to have its integral equal to 1. For instance, for the case of 2D isotropic scattering, it is known that

$$L_{2D}(\rho) \approx \begin{cases} \sqrt{2\pi}\nu_m \rho e^{-\rho^2} & K = 0 \\ \sqrt{2\pi\left(K+1\right)}\rho\nu_m e^{-K-(K+1)\rho^2} I_0\left(2\rho\sqrt{K(K+1)}\right) & K > 0, \end{cases} \tag{49}$$

where $\rho = \frac{R}{\sqrt{\Omega_p}}$ is the envelope signal level normalized by its root-mean square value.

Finally, the average fade duration measures how long, on expectation, the signal envelope will remain below a certain level R. It is known that in general this value can be simply computed as

$$\bar{t}(\rho) = \frac{P\left(\alpha < R\right)}{L_R}, \tag{50}$$

where $P\left(\alpha < R\right)$ is the probability that the signal envelope falls below level R [8]. In that sense, if the fading is assumed to be Rician/Rayleigh, then

$$P\left(\alpha < R\right) \approx \begin{cases} 1 - e^{-\rho^2} & K = 0 \\ 1 - \mathrm{Q}\left(\sqrt{2K}, \sqrt{2(K+1)}\rho\right) & K > 0, \end{cases} \tag{51}$$

where $\mathrm{Q(a, b)}$ is the Marcum Q function.

A. Average Fade Duration with Highly Directional Antenna at Receiver

We now study the AFD for a fading channel with a highly directive antenna at the receiver.

Lemma 3. *Assume that $p(\varphi) = 1/(2\Phi)$, $\varphi \in [-\Phi, \Phi]$, and $G(\varphi) = e^{-k\varphi^2}$. Assume also that $\theta_0 \in [0, \pi]$ and let γ_n and κ_n be defined as*

$$\gamma_n = \Re\left\{\mathrm{erf}\left(\sqrt{k}\frac{\pi}{2} + j\frac{n}{2\sqrt{k}}\right)\right\} e^{-\frac{n^2}{4k}} \tag{52}$$

$$\kappa_n = (2\pi\nu_m)^n \frac{b_0}{\mathrm{erf}\left(\Phi\sqrt{k}\right)}. \tag{53}$$

Then, the coefficients b_1 and b_2 (see Equation 48) can be computed as

$$b_1 = \kappa_1 \left[\gamma_1 - \gamma_0\right] \cos\theta_0 \tag{54}$$

$$b_2 = \kappa_2 \left[\frac{1}{2}\left(\gamma_2 - 2\gamma_1 + \gamma_0\right)\cos 2\theta_0 - \left(\gamma_1 - \gamma_0\right)\right]. \tag{55}$$

The proof is given in Appendix D-A.

Corollary 3.1. *Under the assumptions of Lemma 1 and for highly directive antennas, i.e., $k \gg 1$, the following simplifications can be made:*

$$b_1 = -\frac{b_0}{2k}\pi\nu_m \cos\theta_0 \tag{56}$$

$$b_2 = \frac{2b_0}{k}\left(\pi\nu_m \sin\theta_0\right)^2. \tag{57}$$

The proof follows from approximating Equation 52 using the first order Taylor expansion of $e^{-\frac{n^2}{4k}}$ and substituting the result in Equations 54 and 55, as well as using the equality $1 - \cos(2\theta_0) = 2\sin^2\theta_0$. Note that $b_1 = 0$ if $\theta_0 = \pi/2$. This is expected since any channel with symmetric DPP satisfies this condition [17].

Unfortunately, the AFD for a channel with a generic DPP can only be computed by numerically integrating Equation 47. While this is easily achieved today, it provides little insight as to what is the effect of placing a highly directive antenna on the receiver. To overcome this limitation, we provide three approximations, one for arbitrary θ_0 but applicable only if $b_1/b_2 \ll 1$, $b_1^2/b_2 \ll 1$, another one for $\theta_0 = \pi/2$ and unconstrained b_1 and b_2, and a third one only applicable for a Rayleigh fading channel ($K = 0$).

Lemma 4. *Assume that $p(\varphi) = 1/(2\Phi)$, $\varphi \in [-\Phi, \Phi]$, and $G(\varphi) = e^{-k\varphi^2}$, with $k \gg 1$. Assume also that $\theta_0 \in [0, \pi]$, $b_1/b_2 \ll 1$, $b_1^2/b_2 \ll 1$, and the fading process is Rician-distributed ($K > 0$). Then,*

$$\bar{t}(\rho) \approx \frac{\sqrt{k}}{\sin\theta_0}\bar{t}_{2D}(\rho), \tag{58}$$

where $\bar{t}_{2D}(\rho)$ denotes the average fade duration for the 2D isotropic model estimated using Equations 50, 51. The proof is given in Appendix D-B.

Corollary 4.1. *Assume that $p(\varphi) = 1/(2\Phi)$, $\varphi \in [-\Phi, \Phi]$, and $G(\varphi) = e^{-k\varphi^2}$, with $k \gg 1$. Assume also that the fading process is Rician-distributed and $\theta_0 = \frac{\pi}{2}$. Then,*

$$\bar{t}(\rho) = \sqrt{k} \cdot \bar{t}_{2D}(\rho). \tag{59}$$

The proof follows from Corollary 3.1, particularly the fact that if $\theta_0 = \frac{\pi}{2}$ then $b_1 = 0$. Note that, unlike in Lemma 4, the obtained result is not an approximation but rather the exact value.

Lemma 5. *Assume that $p(\varphi) = 1/(2\Phi)$, $\varphi \in [-\Phi, \Phi]$, and $G(\varphi) = e^{-k\varphi^2}$, with $k \gg 1$. Assume also that the fading process is Rayleigh distributed ($K = 0$) and $\tan\theta_0 > \frac{1}{\sqrt{8k}}$.*

Then,

$$\bar{t}(\rho) = \sqrt{\frac{k}{\sin^2\theta_0 - \frac{1}{8k}\cos^2\theta_0}}\bar{t}_{2D}(\rho). \tag{60}$$

The proof is given in Appendix D-C.

For the case of a 34-m DSN antenna operating at X-band, Equation 60 will therefore only be valid if $\theta_0 > 0.014$ deg.

B. Numerical Results

Figure 8 plots the normalized average fade duration as a function of the fade depth for both Rician and Rayleigh channels. All figures include three plots: the fade duration for a 2D isotropic channel, the fade duration for a 34-m DSN antenna estimated using Equation 58, and the same value computed through numerical integration from Equations 46, 47, and 48, as well as the radiation pattern for a parabolic antenna (Equation 29). Observe that the average fade duration estimated numerically has values close to those predicted by the provided approximations. Indeed, our computational experiments suggest that our approximations provide values that overestimate the AFD by at most a 2x factor. In contrast, the difference between AFD in a downlink from the Moon and the common 2D isotropic model can be three to four orders of magnitude different.

VI. Conclusions

This articles has characterized the time selectivity of a downlink between the South Pole of the Moon and a DSN station assuming that the fading process is uncorrelated and wide-sense stationarity. In particular, we have derived expressions for the Doppler power profile, channel coherence time, and average fade duration as a function of the receiving gain directivity. Results indicate that, for a generic highly directive antenna, the channel will most likely suffer from slow fading, with coherence times inversely proportional to the maximum Doppler shift measured at the DSN station and proportional to the diameter of the receiving dish.

Using orbital propagators, we have shown that the maximum Doppler shift to be expected is as high as 12 kHz approximately, while the angle between the Earth's rotation velocity vector and the LoS direction from transmitter to receiver varies from 75 to 115 deg approximately. Using these facts, together with NASA's frequency allocation at X-band and a 34-meter antenna, we have estimated the channel coherence time to be on the order of 50 msec. Therefore, for a rover transmitting at rates between 1 kbps and 500 kbps, the fading channel observed at the ground receiver will suffer from very slow fading, with blocks of symbols affected by a nearly constant attenuation and phase shift.

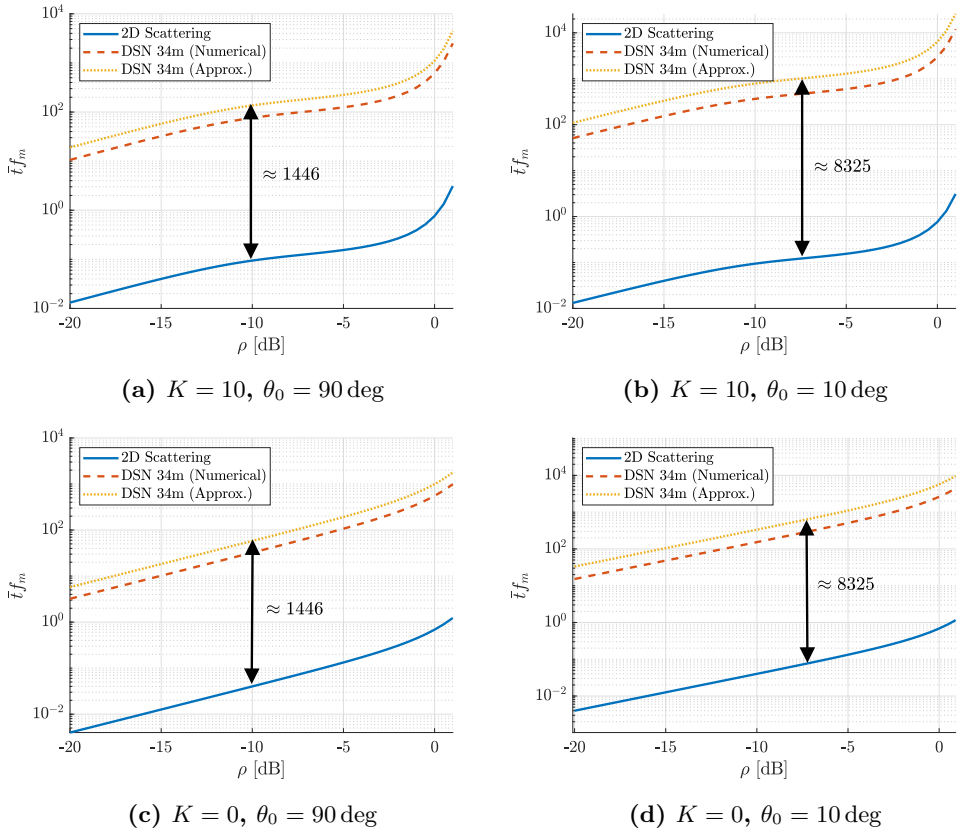

(a) $K = 10$, $\theta_0 = 90\,\text{deg}$ **(b)** $K = 10$, $\theta_0 = 10\,\text{deg}$

(c) $K = 0$, $\theta_0 = 90\,\text{deg}$ **(d)** $K = 0$, $\theta_0 = 10\,\text{deg}$

Figure 8. Average Fade Duration

Finally, characterizing the fading process between the lunar South Pole and a DSN station from a frequency selectivity point-of-view can only be done if delay power profile measurements become available. However, based on Earth-based data from desert-like environments, we have argued that for rovers transmitting tens to hundreds of kilobits per second, the channel is likely to suffer from flat fading effects. That being said, this future research is required to validate this hypothesis.

VII. Acknowledgments

The author is indebted to Dariush Divsalar of the Jet Propulsion Laboratory for his contribution to this work, both during the development and the review phase. Several improvements, additions, and modifications from earlier versions of this document are directly related to his insightful comments.

Appendices

I. Fading Channel Autocorrelation Function with DSN Antenna

A. DSN Antenna Pointed Parallel to the Velocity Vector

We first consider the case where the DSN antenna is pointed almost in the same direction as the velocity vector and assume the conditions from Lemma 1. In that case, we can use the small-angle approximation for the cosine function $\cos\theta = 1 - \frac{\theta^2}{2}$ to re-write the expression for the in-phase component of the channel ACF as

$$\begin{aligned}\phi_{II}^{(s)}(\xi) \approx & b_0 \int_{-\Phi}^{\Phi} \frac{e^{-k\varphi^2}}{\sqrt{\frac{\pi}{k}}\operatorname{erf}\left(\sqrt{k}\Phi\right)} \cos\left(2\pi\xi\left[1-\frac{(\theta_0+\varphi)^2}{2}\right]\right) d\varphi \\ = & \frac{b_0}{\operatorname{erf}\left(\sqrt{k}\Phi\right)}\sqrt{\frac{k}{\pi}}\Re\int_{-\Phi}^{\Phi} e^{-k\varphi^2+j2\pi\xi\left[1-\frac{(\theta_0+\varphi)^2}{2}\right]} d\varphi \\ = & \frac{b_0}{\operatorname{erf}\left(\sqrt{k}\Phi\right)}\sqrt{\frac{k}{\pi}}\Re\left\{e^{j2\pi\xi}\int_{-\Phi}^{\Phi} e^{-k\varphi^2-j\pi\xi(\theta_0+\varphi)^2} d\varphi\right\}.\end{aligned} \tag{61}$$

Similarly, the cross-correlation between the in-phase and quadrature components will be

$$\begin{aligned}\phi_{IQ}^{(s)}(\xi) \approx & b_0 \int_{-\Phi}^{\Phi} \frac{e^{-k\varphi^2}}{\sqrt{\frac{\pi}{k}}\operatorname{erf}\left(\sqrt{k}\Phi\right)} \sin\left(2\pi\xi\left[1-\frac{(\theta_0+\varphi)^2}{2}\right]\right) d\varphi \\ = & b_0 \int_{-\Phi}^{\Phi} \frac{e^{-k\varphi^2}}{\sqrt{\frac{\pi}{k}}\operatorname{erf}\left(\sqrt{k}\Phi\right)} \cos\left(2\pi\xi\left[1-\frac{(\theta_0+\varphi)^2}{2}\right]-\frac{\pi}{2}\right) d\varphi \\ = & \frac{b_0}{\operatorname{erf}\left(\sqrt{k}\Phi\right)}\sqrt{\frac{k}{\pi}}\Re\left\{e^{j\left(2\pi\xi-\frac{\pi}{2}\right)}\int_{-\Phi}^{\Phi} e^{-k\varphi^2-j\pi\xi(\theta_0+\varphi)^2} d\varphi\right\}.\end{aligned} \tag{62}$$

Solving the integral

$$\kappa(\xi) = \int e^{-k\varphi^2-j\pi\xi(\theta_0+\varphi)^2} d\varphi \tag{63}$$

involves completing the square form in the integrand's exponent and making a change of variable such that the resulting expression resembles the Error function. For instance, let

$$u = \frac{k\varphi + j\pi\xi(\varphi+\theta_0)}{\sqrt{k+j\pi\xi}}. \tag{64}$$

Then, some algebra will yield

$$\begin{aligned}\kappa(\xi) = & \frac{1}{2}\sqrt{\frac{\pi}{k+j\pi\xi}} e^{-\frac{(\pi\theta_0\xi)^2}{k+j\pi\xi}-j\pi\xi\theta_0^2}\int\frac{2e^{-u^2}}{\sqrt{\pi}}du \\ = & \frac{1}{2}\sqrt{\frac{\pi}{k+j\pi\xi}} e^{-\frac{(\pi\theta_0\xi)^2}{k+j\pi\xi}-j\pi\xi\theta_0^2}\operatorname{erf} u.\end{aligned} \tag{65}$$

Next, we assume that $k \gg 1$ such that $k \gg \pi\xi$. Then

$$\operatorname{erf} u \approx \operatorname{erf}\left(\sqrt{k}\varphi + j\frac{\pi\xi(\varphi+\theta_0)}{\sqrt{k}}\right) \approx \operatorname{erf}\left(\sqrt{k}\varphi\right), \tag{66}$$

which results in

$$\kappa(\xi) \approx \frac{1}{2}\sqrt{\frac{\pi}{k}} e^{-\frac{(\pi\theta_0\xi)^2}{k} - j\pi\xi\theta_0^2} \operatorname{erf}\left(\sqrt{k}\varphi\right), \tag{67}$$

and therefore

$$\int_{-\Phi}^{\Phi} e^{-k\varphi^2 - j\pi\xi(\theta_0+\varphi)^2} d\varphi \approx \sqrt{\frac{\pi}{k}} e^{-\frac{(\pi\theta_0\xi)^2}{k} - j\pi\xi\theta_0^2}. \tag{68}$$

In this last expression we have assumed once again that $k \gg 1$ so that $\operatorname{erf}\left(\pm\sqrt{k}\Phi\right) \approx \pm 1$. Furthermore,

$$\begin{aligned}
\phi_{II}^{(s)}(\xi) \approx & b_0\sqrt{\frac{k}{\pi}}\Re\left\{e^{j2\pi\xi}\sqrt{\frac{\pi}{k}}e^{-\frac{(\pi\theta_0\xi)^2}{k} - j\pi\xi\theta_0^2}\right\} \\
= & b_0 e^{-\frac{(\pi\theta_0\xi)^2}{k}}\Re\left\{e^{j\pi\xi(2-\theta_0^2)}\right\} \\
= & b_0 e^{-\frac{(\pi\theta_0\xi)^2}{k}}\cos\left(2\pi\xi\left[1-\frac{\theta_0^2}{2}\right]\right) \\
\approx & b_0 e^{-\frac{(\pi\theta_0\xi)^2}{k}}\cos(2\pi\xi\cos\theta_0).
\end{aligned} \tag{69}$$

Similarly,

$$\begin{aligned}
\phi_{IQ}^{(s)}(\xi) \approx & b_0 e^{-\frac{(\pi\theta_0\xi)^2}{k}}\Re\left\{e^{j\pi\xi(2-\theta_0^2)-\frac{\pi}{2}}\right\} \\
= & b_0 e^{-\frac{(\pi\theta_0\xi)^2}{k}}\cos\left(2\pi\xi\left[1-\frac{\theta_0^2}{2}\right]-\frac{\pi}{2}\right) \\
\approx & b_0 e^{-\frac{(\pi\theta_0\xi)^2}{k}}\sin(2\pi\xi\cos\theta_0).
\end{aligned} \tag{70}$$

Finally,

$$\begin{aligned}
\phi_{rr}^{(s)}(\xi) = & \phi_{II}^{(s)}(\xi) + j\phi_{IQ}^{(s)}(\xi) \\
= & b_0 e^{-\frac{(\pi\theta_0\xi)^2}{k}}\left[\cos(2\pi\xi\cos\theta_0) + j\sin(2\pi\xi\cos\theta_0)\right] \\
= & b_0 e^{-\frac{(\pi\theta_0\xi)^2}{k} + j2\pi\xi\cos\theta_0}.
\end{aligned} \tag{71}$$

B. DSN Antenna Pointed Perpendicular to the Velocity Vector

We now consider the case where the DSN antenna is pointed almost perpendicular to the velocity vector and, once again, accept the assumptions stated in Lemma 1. Define the angle ϵ as the difference between the actual DSN pointing direction and the normal to the velocity vector: $\epsilon \triangleq \frac{\pi}{2} - \theta_0$. Then, the in-phase component of the fading

channel ACF can be expressed as

$$\begin{aligned}\phi_{II}^{(s)}(\xi) =& b_0 \int_{-\Phi}^{\Phi} \frac{e^{-k\varphi^2}}{\sqrt{\frac{\pi}{k}}\operatorname{erf}\left(\sqrt{k}\Phi\right)} \cos\left(2\pi\xi\cos\left[\frac{\pi}{2}-\epsilon+\varphi\right]\right) d\varphi \\ =& \frac{b_0}{\operatorname{erf}\left(\sqrt{k}\Phi\right)}\sqrt{\frac{k}{\pi}} \int_{-\Phi}^{\Phi} e^{-k\varphi^2} \cos\left(2\pi\xi\sin\left[\epsilon+\varphi\right]\right) d\varphi \\ \approx& \frac{b_0}{\operatorname{erf}\left(\sqrt{k}\Phi\right)}\sqrt{\frac{k}{\pi}} \int_{-\Phi}^{\Phi} e^{-k\varphi^2} \cos\left(2\pi\xi\left[\epsilon+\varphi\right]\right) d\varphi \\ =& \frac{b_0}{\operatorname{erf}\left(\sqrt{k}\Phi\right)}\sqrt{\frac{k}{\pi}} \Re\left\{ e^{j2\pi\xi\epsilon} \int_{-\Phi}^{\Phi} e^{-k\varphi^2+j2\pi\xi\varphi} d\varphi \right\}.\end{aligned} \tag{72}$$

Note that in Equation 72 we have used the small-angle approximation for the sine function, $\sin\theta \approx \theta$. Similarly,

$$\phi_{IQ}^{(s)}(\xi) = \frac{b_0}{\operatorname{erf}\left(\sqrt{k}\Phi\right)}\sqrt{\frac{k}{\pi}} \Re\left\{ e^{j\left(2\pi\xi\epsilon-\frac{\pi}{2}\right)} \int_{-\Phi}^{\Phi} e^{-k\varphi^2+j2\pi\xi\varphi} d\varphi \right\}. \tag{73}$$

To solve the integral

$$\kappa(\xi) = \int e^{-k\varphi^2+j\pi\xi\varphi} d\varphi, \tag{74}$$

we follow a similar procedure to the one outlined in the previous section; i.e we complete the square of the integrand's exponent and then apply the substitution

$$u = \frac{k\varphi - j\pi\xi}{\sqrt{k}}, \tag{75}$$

which results in

$$\begin{aligned}\kappa(\xi) =& \frac{1}{2}\sqrt{\frac{\pi}{k}} e^{-\frac{(\pi\xi)^2}{k}} \int \frac{2e^{-u^2}}{\sqrt{\pi}} d\varphi \\ =& \frac{1}{2}\sqrt{\frac{\pi}{k}} e^{-\frac{(\pi\xi)^2}{k}} \operatorname{erf} u.\end{aligned} \tag{76}$$

Next, we assume that $k \gg 1$ which results in

$$\operatorname{erf} u \approx \operatorname{erf}\left(\sqrt{k}\varphi - j\frac{\pi\xi}{\sqrt{k}}\right) \approx \operatorname{erf}\left(\sqrt{k}\varphi\right), \tag{77}$$

and therefore

$$\int_{-\Phi}^{\Phi} e^{-k\varphi^2+j2\pi\xi\varphi} d\varphi \approx \sqrt{\frac{\pi}{k}} e^{-\frac{(\pi\xi)^2}{k}}. \tag{78}$$

In this last expression we have assumed once again that $k \gg 1$ so that $\operatorname{erf}\left(\pm\sqrt{k}\Phi\right) \approx \pm 1$. Furthermore, direct substitution in the previous equations for

$\phi_{II}^{(s)}(\xi)$ and $\phi_{IQ}^{(s)}(\xi)$ yields

$$\begin{aligned}\phi_{II}^{(s)}(\xi) =& b_0\sqrt{\frac{k}{\pi}}\Re\left\{e^{j2\pi\xi\epsilon}\sqrt{\frac{\pi}{k}}e^{-\frac{(\pi\xi)^2}{k}}\right\}\\ =& b_0 e^{-\frac{(\pi\xi)^2}{k}}\cos(2\pi\xi\epsilon)\\ =& b_0 e^{-\frac{(\pi\xi)^2}{k}}\cos(2\pi\xi\left[\frac{\pi}{2}-\theta_0\right])\\ \approx& b_0 e^{-\frac{(\pi\xi)^2}{k}}\cos(2\pi\xi\cos\theta_0)\end{aligned} \tag{79}$$

and

$$\begin{aligned}\phi_{IQ}^{(s)}(\xi) =& b_0\sqrt{\frac{k}{\pi}}\Re\left\{e^{j\left(2\pi\xi\epsilon-\frac{\pi}{2}\right)}\sqrt{\frac{\pi}{k}}e^{-\frac{(\pi\xi)^2}{k}}\right\}\\ \approx& b_0 e^{-\frac{(\pi\xi)^2}{k}}\sin(2\pi\xi\cos\theta_0),\end{aligned} \tag{80}$$

where we have used the small angle approximation as follows:

$$\cos\theta_0 = \cos\left(\frac{\pi}{2}-\epsilon\right) = \sin\epsilon \approx \epsilon \triangleq \frac{\pi}{2}-\theta_0. \tag{81}$$

Finally,

$$\begin{aligned}\phi_{rr}^{(s)}(\xi) =& \phi_{II}^{(s)}(\xi) + j\phi_{IQ}^{(s)}(\xi)\\ =& b_0 e^{-\frac{(\pi\xi)^2}{k}}\left[\cos(2\pi\xi\cos\theta_0) + j\sin(2\pi\xi\cos\theta_0)\right]\\ =& b_0 e^{-\frac{(\pi\xi)^2}{k}+j2\pi\xi\cos\theta_0}.\end{aligned} \tag{82}$$

II. Fading Channel Doppler Power Profile with DSN Antenna

A. DSN Antenna Pointed Parallel to the Velocity Vector

In this appendix we derive the DPP for the fading channel with the DSN antenna assuming high antenna directivity, i.e., $k \gg 1$. For the case where $\theta_0 \to 0$ we have

$$\begin{aligned}S_{rr}^{(s)}(f) \approx& b_0\mathcal{F}\left\{e^{-\frac{(\pi\theta_0\xi)^2}{k}+j2\pi\xi\cos\theta_0}\right\}\\ =& b_0\mathcal{F}\left\{e^{-\frac{(\pi\theta_0\xi)^2}{k}}\right\} * \mathcal{F}\left\{e^{j2\pi\xi\cos\theta_0}\right\}.\end{aligned} \tag{83}$$

The first Fourier transform is just a scaled Gaussian function. Therefore, using the fact that

$$ae^{-\pi(ax)^2} \overset{\mathcal{F}}{\longleftrightarrow} e^{-\pi\left(\frac{f}{a}\right)^2} \tag{84}$$

we get

$$e^{-\frac{(\pi\theta_0\xi)^2}{k}} \overset{\mathcal{F}}{\longleftrightarrow} \sqrt{\frac{k}{\pi}}\frac{1}{\theta_0}e^{-\frac{k}{\theta_0^2}f^2}. \tag{85}$$

The second Fourier transform is also immediate to compute and results in

$$e^{j2\pi\xi\cos\theta_0} \overset{\mathcal{F}}{\longleftrightarrow} \delta(f-\cos\theta_0). \tag{86}$$

Finally, note that the right-hand side of Equation 85 is not well-defined for $\theta_0 = 0$. However, if you make the appropriate substitution in Equation 32, it is straightforward to prove the result in Equation 33 using Equation 86.

B. DSN Antenna Pointed Perpendicular to the Velocity Vector

For $k \gg 1$ and $\theta_0 \to \frac{\pi}{2}$ we have

$$\begin{aligned} S_{rr}^{(s)}(f) \approx & b_0 \mathcal{F}\left\{ e^{-\frac{(\pi\xi)^2}{k} + j2\pi\xi\cos\theta_0} \right\} \\ = & b_0 \mathcal{F}\left\{ e^{-\frac{(\pi\xi)^2}{k}} \right\} * \mathcal{F}\left\{ e^{j2\pi\xi\cos\theta_0} \right\}. \end{aligned} \tag{87}$$

The expression in Equation 33 can be obtained by applying the same reasoning as before.

III. Fading Channel Coherence Time with DSN Antenna

The channel coherence time can be estimated as $T_c = \frac{1}{\sigma_\nu}$, where σ_ν^2 is the Doppler spread:

$$\sigma_\nu^2 = b_0 \int_{-\infty}^{\infty} (\nu - \bar{\nu})^2 C_{h_2}(\nu) d\nu, \tag{88}$$

where

$$\bar{\nu} = b_0 \int_{-\infty}^{\infty} \nu C_{h_2}(\nu) d\nu. \tag{89}$$

In the case of the a DSN antenna at the receiver, it is immediately seen that $\bar{\nu} = \nu\cos\theta_0$. Consequently,

$$\begin{aligned} \sigma_\nu^2 = & b_0 \int_{-\infty}^{\infty} (\nu - \nu_m\cos\theta_0)^2 \frac{b_0}{\nu_m c}\sqrt{\frac{k}{\pi}} e^{-\frac{k}{c^2}\left(\frac{\nu}{\nu_m} - \cos\theta_0\right)^2} d\nu \\ = & \frac{\nu_m^2}{c}\sqrt{\frac{k}{\pi}} \int_{-\infty}^{\infty} (f - \cos\theta_0)^2 e^{-\frac{k}{c^2}(f - \cos\theta_0)^2} df, \end{aligned} \tag{90}$$

where $c = 1$ if $\theta_0 \to \frac{\pi}{2}$ and $c = \theta_0$ if $\theta_0 \to 0$, and we have applied the change of variables $f = \nu/\nu_m$. Solving the integral yields

$$\sigma_\nu^2 = \frac{(\nu_m c)^2}{2k}, \tag{91}$$

and therefore

$$T_c = \frac{\sqrt{2k}}{\nu_m c}. \tag{92}$$

IV. Fading Channel AFD with DSN Antenna

A. Derivation of constants b_1, b_2 for DSN Antenna

Let us define the following integral:

$$\kappa_n = \int_{-\Phi}^{\Phi} \frac{e^{-k\varphi^2}}{\sqrt{\frac{\pi}{k}}\operatorname{erf}\left(\sqrt{k}\Phi\right)} \cos^n(\varphi+\theta_0). \tag{93}$$

Then, using arguments analogous to Appendix A, we can prove that

$$\kappa_0 = 1 \tag{94}$$

$$\kappa_1 = \frac{1}{\operatorname{erf}\left(\sqrt{k}\Phi\right)} \Re\left\{\operatorname{erf}\left(\sqrt{k}\Phi + \frac{j}{2\sqrt{k}}\right)\right\} e^{-\frac{1}{4k}} \cos\theta_0 \tag{95}$$

$$\kappa_2 = \frac{1}{2\operatorname{erf}\left(\sqrt{k}\Phi\right)} \left[1 + \Re\left\{\operatorname{erf}\left(\sqrt{k}\Phi + \frac{j}{\sqrt{k}}\right)\right\} e^{-\frac{1}{k}} \cos 2\theta_0\right]. \tag{96}$$

Furthermore, if $k \gg 1$, then

$$\kappa_0 = 1 \tag{97}$$

$$\kappa_1 = e^{-\frac{1}{4k}} \cos\theta_0 \tag{98}$$

$$\kappa_2 = \frac{1}{2}\left[1 + e^{-\frac{1}{k}} \cos 2\theta_0\right]. \tag{99}$$

From Equation 48 and using the change of variables $\varphi = \theta - \theta_0$ we know that

$$b_n = (2\pi\nu_m)^n \int_{-\Phi}^{\Phi} \frac{e^{-k\varphi^2}}{\sqrt{\frac{\pi}{k}}\operatorname{erf}\left(\sqrt{k}\Phi\right)} \left[\cos(\varphi+\theta_0) - \cos\theta_0\right]^n d\varphi, \tag{100}$$

Then, it is immediately seen that

$$b_1 = (2\pi\nu_m) b_0 \left[\kappa_1 - \kappa_0 \cos\theta_0\right] \tag{101}$$

$$b_2 = (2\pi\nu_m)^2 b_0 \left[\kappa_2 - 2\kappa_1 \cos\theta_0 + \kappa_0 \cos^2\theta_0\right]. \tag{102}$$

which results in

$$b_1 = (2\pi\nu_m) b_0 \left[e^{-\frac{1}{4k}} - 1\right] \cos\theta_0 \tag{103}$$

$$b_2 = (2\pi\nu_m)^2 b_0 \left[\frac{1}{2}\left(e^{-\frac{1}{k}} - 2e^{-\frac{1}{4k}} + 1\right)\cos 2\theta_0 - \left(e^{-\frac{1}{4k}} - 1\right)\right]. \tag{104}$$

Finally, let $\gamma_n = e^{-\frac{n^2}{4k}}$. Then,

$$b_1 = (2\pi\nu_m) b_0 \left[\gamma_1 - \gamma_0\right] \cos\theta_0 \tag{105}$$

$$b_2 = (2\pi\nu_m)^2 b_0 \left[\frac{1}{2}\left(\gamma_2 - 2\gamma_1 + \gamma_0\right)\cos 2\theta_0 - \left(\gamma_1 - \gamma_0\right)\right]. \tag{106}$$

B. Derivation of AFD for Rician Channel

It is known that for any given fading channel, the level crossing rate is given by

$$L_R = \int_0^\infty \dot{\alpha} p(\alpha = R, \dot{\alpha}) d\dot{\alpha}, \tag{107}$$

where

$$p(\alpha, \dot{\alpha}) = \frac{\alpha (2\pi)^{-3/2}}{\sqrt{B b_0}} \int_\pi^{-\pi} \exp\left[-\frac{B\left(\alpha^2 - 2\alpha s \cos\psi + s^2\right) + \left(b_0 \dot{\alpha} + b_1 s \sin\psi\right)^2}{2 B b_0} \right] d\psi, \tag{108}$$

Assume that $b_1/b_2 \ll 1$ and $b_1^2/b_2 \ll 1$. Then, $B = b_0 b_2 - b_1^2 \approx b_0 b_2$ and we can expand the square form inside the integrand. Taking all terms that do not depend on ψ out of the equation, we get

$$\begin{aligned} p(\alpha, \dot{\alpha}) =& \frac{(2\pi)^{-3/2}}{\sqrt{b_2 b_0}} \frac{\alpha}{\sqrt{b_0}} e^{-\frac{\alpha^2 + s^2}{2 b_0}} e^{-\frac{\dot{\alpha}^2}{2 b_2}} \int_{-\pi}^{\pi} \exp\left[\frac{\alpha s \cos\psi}{b_0} - \frac{b_1^2}{b_2} \frac{s^2 \sin^2\psi}{2 b_0} + \frac{b_1}{b_2} \dot{\alpha} s \sin\psi \right] d\psi \\ \approx& \frac{(2\pi)^{-3/2}}{\sqrt{b_2 b_0}} \frac{\alpha}{\sqrt{b_0}} e^{-\frac{\alpha^2 + s^2}{2 b_0}} e^{-\frac{\dot{\alpha}^2}{2 b_2}} \int_{-\pi}^{\pi} e^{\frac{\alpha s \cos\psi}{b_0}} d\psi. \end{aligned} \tag{109}$$

Consequently,

$$\begin{aligned} L_R \approx& \frac{(2\pi)^{-3/2}}{\sqrt{b_2 b_0}} \frac{\alpha}{\sqrt{b_0}} e^{-\frac{\alpha^2 + s^2}{2 b_0}} I_0\left(\frac{\alpha s}{b_0}\right) \int_0^\infty \dot{\alpha} e^{-\frac{\dot{\alpha}^2}{2 b_2}} d\dot{\alpha} \\ =& \sqrt{\frac{b_2}{2\pi b_0}} \frac{\alpha}{\sqrt{b_0}} e^{-\frac{\alpha^2 + s^2}{2 b_0}} I_0\left(\frac{\alpha s}{b_0}\right). \end{aligned} \tag{110}$$

Define $\rho = \frac{\alpha}{\sqrt{s^2 + 2 b_0}}$ and $K = \frac{s^2}{2 b_0}$. Then

$$L_R \approx \sqrt{\frac{b_2}{\pi b_0}} \sqrt{K+1} \rho e^{-K - (K+1)\rho^2} I_0\left(2\rho\sqrt{K(K+1)}\right). \tag{111}$$

Observe that in this last equation only b_2 depends on the type of channel under consideration. Therefore, the ratio between level crossing rates for two different channels is simply

$$\frac{L_{R,ch1}}{L_{R,ch2}} = \sqrt{\frac{b_{2,ch1}}{b_{2,ch2}}}. \tag{112}$$

Moreover, since the AFD is inversely proportional to the level crossing rate,

$$\frac{\bar{t}_{ch1}}{\bar{t}_{ch2}} = \sqrt{\frac{b_{2,ch2}}{b_{2,ch1}}}. \tag{113}$$

Let $ch2$ be a 2D isotropic scattering channel with arbitrary K and $\theta_0 = \pi/2$. Then, it is known that $b_1 = 0$ and $b_2 = 2\left(\pi\nu_m\right)^2 b_0$ since the DPP is symmetric. Assume that channel $ch1$ satisfies the conditions of Corollary 3.1. Then, using Equation 57 it is immediately shown that

$$\frac{\bar{t}_{DSN}}{\bar{t}_{2D}} \approx \frac{\sqrt{k}}{\sin\theta_0}. \tag{114}$$

Note that this approximation is only valid if $b_1/b_2 \ll 1$ and $b_1^2/b_2 \ll 1$. Using the results from Corollary 3.1, have

$$\frac{b_1}{b_2} = \frac{1}{4\pi f_m}\frac{\cot\theta_0}{\sin\theta_0} \tag{115}$$

$$\frac{b_1^2}{b_2} = \frac{b_0}{8k}\cot^2\theta_0. \tag{116}$$

Therefore, given that $\nu_m \gg 1$ and $k \gg 1$, these conditions will be met for all angles except for θ_0, in the vicinity of zero. Indeed, we have seen that the fading channel DPP degenerates to a delta if $\theta_0 = 0$ and therefore the average fade duration tends to infinity.

C. Derivation of AFD for Rayleigh Channel

Under the assumption of Rayleigh fading it is known that the level crossing rate of the fading process can be computed as [8], pp. 119,

$$L(\rho) = \sqrt{\frac{b_2}{b_0} - \frac{b_1^2}{b_0^2}}\frac{\rho}{\sqrt{\pi}}e^{-\rho^2} = \varsigma\frac{\rho}{\sqrt{\pi}}e^{-\rho^2}. \tag{117}$$

Consequently,

$$\frac{\bar{t}_{ch1}}{\bar{t}_{ch2}} = \frac{\varsigma_{ch2}}{\varsigma_{ch1}}. \tag{118}$$

For a fading channel with 2D isotropic scattering, $\varsigma_{2D} = \sqrt{2}\pi\nu_m$ (see Equation 49). Alternatively, for a highly directive antenna like the DSN 34-meter dishes we have

$$\varsigma_{DSN} = \sqrt{2}\pi f_m\sqrt{\frac{1}{k}\sin^2\theta_0 - \frac{1}{8k^2}\cos^2\theta_0}. \tag{119}$$

Therefore,

$$\frac{\bar{t}_{DSN}}{\bar{t}_{2D}} = \frac{\varsigma_{2D}}{\varsigma_{DSN}} = \sqrt{\frac{k}{\sin^2\theta_0 - \frac{1}{8k}\cos^2\theta_0}}. \tag{120}$$

Note that this result is only valid if the denominator of the right-hand side of Equation 120 is positive so that its square root is not imaginary. Consequently, $\tan\theta_0 > \frac{1}{\sqrt{8k}}$ must hold.

References

[1] D. R. Andrews, A. Colaprete, J. Quinn, D. Chavers, and M. Picard, "Introducing the resource prospector (RP) mission," in *AIAA SPACE 2014 Conference and Exposition*, 2014, p. 4378.

[2] J. N. Goswami and M. Annadurai, "Chandrayaan-2 mission," in *Lunar and Planetary Science Conference*, vol. 42, 2011, p. 2042.

[3] M. Angert, P. Malouf, C. Spouse, and R. Awadallah, "Summary of international lunar network multipath models and simulations," Johns Hopkins APL, Tech. Rep. IQJ01360, March 2010.

[4] Communications and Sensor Systems Department, "Lunar multipath signal characteristics," NATIONAL AERONAUTICS AND SPACE ADMINISTRATION, Tech. Rep. NAS 9-8166, 1969.

[5] Y. C. Loh, J. Boster, S. Hwu, J. Watson, and K. De Silva, "Wireless video system for extra vehicular activity in the international space station and space shuttle orbiter environment," in *Vehicular Technology Conference, 1999 IEEE 49th*, vol. 2. IEEE, 1999, pp. 1203–1206.

[6] Flight Communications Systems Section, "MER-A EDL: 16 minute lack of received signal post landing," Jet Propulsion Laboratory, Tech. Rep., 2004.

[7] R. M. Gutierrez, H. Yu, Y. Rong, and D. W. Bliss, "Time and frequency dispersion characteristics of the UAS wireless channel in residential and mountainous desert terrains," in *Consumer Communications & Networking Conference (CCNC), 2017 14th IEEE Annual*. IEEE, 2017, pp. 516–521.

[8] G. L. Stüber, *Principles of mobile communication*, 2nd ed. Springer, 1996.

[9] G. Matz and F. Hlawatsch, "Fundamentals of time-varying communication channels," in *Wireless Communications over Rapidly Time-Varying Channels*. Elsevier, 2011, pp. 1–63.

[10] A. Paier, J. Karedal, N. Czink, C. Dumard, T. Zemen, F. Tufvesson, A. F. Molisch, and C. F. Mecklenbräuker, "Characterization of vehicle-to-vehicle radio channels from measurements at 5.2 GHz," *Wireless personal communications*, vol. 50, no. 1, pp. 19–32, 2009.

[11] 3rd Generation Partnership Project, "Technical specification group radio access network; deployment aspects," 3rd Generation Partnership Project, Tech. Rep. 3GPP TR 25.943, April 2011.

[12] European Telecommunications Standards Institute, "Study on channel model for frequency spectrum above 6 GHz," European Telecommunications Standards Institute, Tech. Rep. TR 138 900 V14.2.0, June 2017.

[13] V. Jamnejad, "A study of near to far fields of JPL deep space network (DSN) antennas for RFI analysis," in *Aerospace Conference, 2004. Proceedings. 2004 IEEE*, vol. 2. IEEE, 2004, pp. 975–986.

[14] ITU Radiocommunication Sector, "Mathematical model of average radiation patterns for line-of-sight point-to-point radio-relay system antennas for use in certain coordination studies and interference assessment in the frequency range from 1 to about 40 GHz," ITU Radiocommunication Sector, Tech. Rep. F.1245, 1997.

[15] Jet Propulsion Laboratory, "34-m BWG stations telecommunications interfaces," Jet Propulsion Laboratory, Tech. Rep. 810-005, 104, Rev. J, 2017.

[16] G. Maral and M. Bousquet, *Satellite communications systems: systems, techniques and technology*. John Wiley & Sons, 2011.

[17] S. O. Rice, "Statistical properties of a sine wave plus random noise," *Bell System Technical Journal*, vol. 27, no. 1, pp. 109–157, 1948.